



HAL
open science

Tolerance analysis of photonic crystal substrate used in spectrometer-free photonic crystal enhanced microscopy

Young-Gu Ju

► **To cite this version:**

Young-Gu Ju. Tolerance analysis of photonic crystal substrate used in spectrometer-free photonic crystal enhanced microscopy. 2023. hal-03953359

HAL Id: hal-03953359

<https://hal.science/hal-03953359>

Preprint submitted on 24 Jan 2023

HAL is a multi-disciplinary open access archive for the deposit and dissemination of scientific research documents, whether they are published or not. The documents may come from teaching and research institutions in France or abroad, or from public or private research centers.

L'archive ouverte pluridisciplinaire **HAL**, est destinée au dépôt et à la diffusion de documents scientifiques de niveau recherche, publiés ou non, émanant des établissements d'enseignement et de recherche français ou étrangers, des laboratoires publics ou privés.

Tolerance analysis of photonic crystal substrate used in spectrometer-free photonic crystal enhanced microscopy

Young-Gu Ju

Department of Physics Education, Kyungpook National University,
80 Daehakro, Bukgu, Daegu 41566, Korea
E-mail: ygju@knu.ac.kr

Abstract

We performed a tolerance analysis of a photonic crystal (PC) substrate used in spectrometer-free photonic crystal enhanced microscopy (SFPCEM). SFPCEM is a simplified version of photonic crystal enhanced microscopy and is used for viewing nanoparticles without an expensive spectrometer or a scanning stage. We varied various structural parameters of the PC substrate and determined the change in its spectral behavior in order to find out the tolerance and sensitivity of its final performance to the parameters. We also analyzed the incident light angle dependency of the PC substrate, and in an SFPCEM observation of a nanoparticle, it caused the image of a nanoparticle to be stretched. The tolerance analysis may help to optimize the PC substrate for observing nanoparticles more clearly in SFPCEM and provides the permissible fabrication error boundary for reasonable performance.

1. Introduction

Recently, nanoparticles made of dielectric, semiconductor, metal, and magnetic materials have been vigorously studied and their applications are becoming increasingly important [1–4]. The detection of a target molecule by attaching a ligand to a nanoparticle and interacting with electromagnetic wave is a very useful and valuable tool in the field of biosensing [5–7]. In particular, a nanoparticle with a permittivity greater than that of water can be used for increasing a biosensing signal and as a secondary tag. Furthermore, the magnetic attraction of magnetic nanoparticles can assist the movement and the handling of the nanoparticles [8]. Metal nanoparticles of silver or gold can generate surface plasmons under external illumination and can show a strong localized electromagnetic field on their surface [9, 10]. Several biosensing methods are available for detecting the adsorption of nanoparticles on a specific active area [11, 12]. However, it is not easy to guide nanoparticles to the specific area. Some researchers have attempted to use an imaging detection method in which the entire substrate is activated instead of a specific area, thereby increasing the field of view (FOV) significantly compared with nonimaging methods. Imaging-based biosensing methods include surface plasmon resonance sensors [13], photonic crystal (PC) biosensors [14], and dielectric film interference sensors [15]. The very small change in permittivity caused by the analyte facilitates the observation of target molecules.

Photonic crystal enhanced microscopy (PCEM) can be used for imaging dielectric or metal nanoparticles attached to a PC surface. In general, it is very difficult to view the nanoparticles with an optical microscope. In PCEM, nanoparticles change the reflectivity of the PC considerably at the resonance wavelength by disturbing the evanescent wave formed on the surface of the PC. The microscope used for PCEM is a special optical microscope optimized for imaging and detecting changes caused by the nanoparticles and amplified by the PC. A recent publication reported the feasibility of detecting a single nanoparticle by using PCEM and the possibility of using the technique

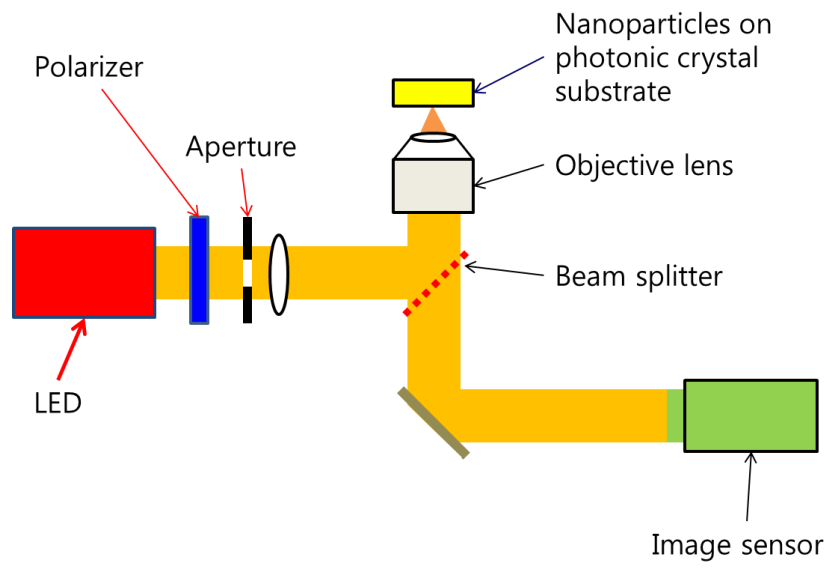
as a potent biosensing tool [16, 17]. In spite of its excellent performance, the present PCEM equipment involves a high-performance spectrometer, a precision scanning stage, and a fiber-coupled light source, which increase the price of the equipment up to about \$100,000. The use of the line scan method with an expensive spectrometer may hinder the expansion of the range of applications to applications such as point-of-care (POC) applications. In particular, the line scan method is slow in acquiring images and provides a very small FOV, which may decrease the speed and efficiency of analyzing a sample.

In order to overcome this problem, we propose a modified PCEM technique that does not involve a spectrometer or the line scan method. This technique gets rid of expensive parts, and the ensuing signal loss is compensated for by superior image processing. The simplification of hardware and improvement of image processing provide several advantages such as low production cost, a high image acquisition speed, and a large FOV.

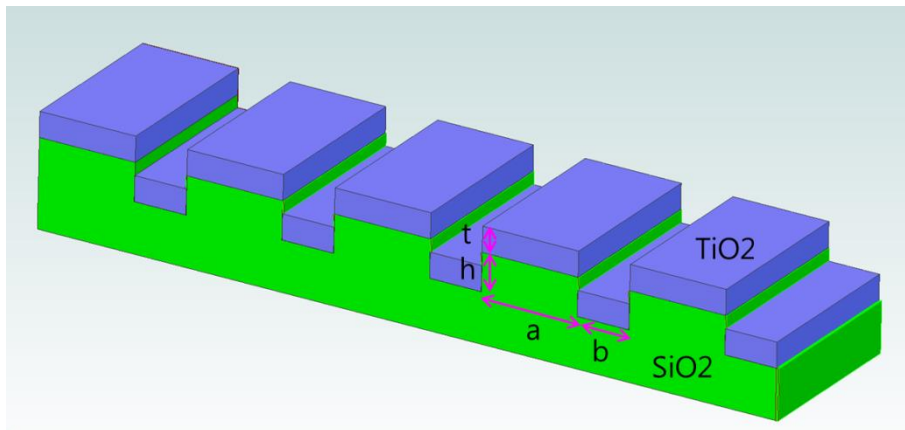
In this study, we conducted a tolerance analysis of a PC substrate used for spectrometer-free PCEM (SFPCEM). We determined the spectral behavior of the PC substrate associated with a change in the structural parameters of the substrate. Furthermore, the incident light angle dependency of the PC substrate, which showed spectral changes at various incidence angles, was examined. We explain how this incident light angle dependency affects the image of nanoparticles in SFPCEM. The tolerance analysis may be helpful for fabricating PC substrates for SFPCEM for observing nanoparticles in with higher contrast, and framing guidelines for the fabrication error of the PC substrate.

2. Simulations

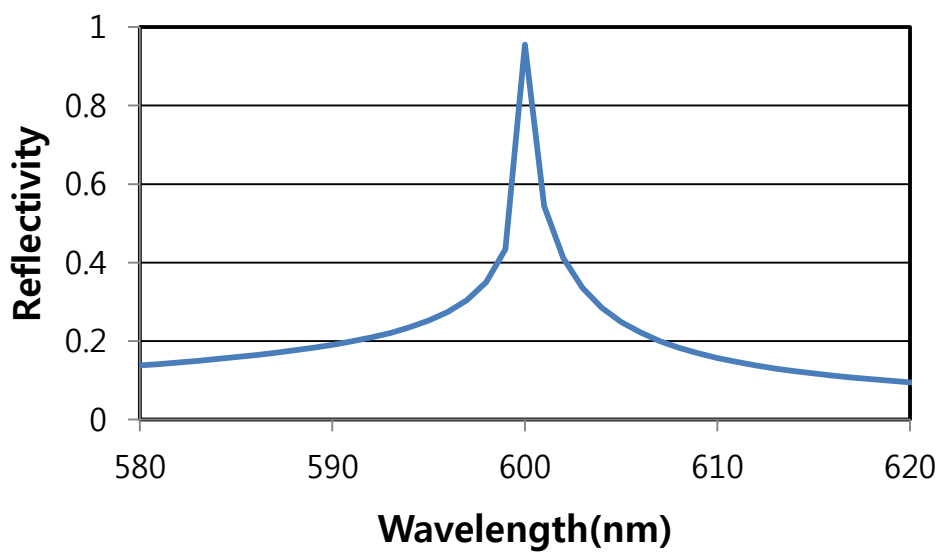
The tolerance analysis of a PC substrate used in SFPCEM requires an understanding of SFPCEM. A schematic of SFPCEM is presented in Fig. 1(a). The optical setup for SFPCEM is similar to that of a typical epi-illumination microscope, except for the light source being polarized and the collimated light-emitting diode (LED) and sample being mounted on a PC instead of a glass substrate. The PC substrate provides enhanced image contrast for Au nanoparticles since its high reflectivity at the resonance wavelength drops drastically when Au nanoparticles are present on it. A typical structure of a PC substrate is shown in Fig. 1(b). The PC substrate used in PCEM is basically a coated dielectric grating that exhibits sharp resonance (Fig. 1(c)). The sharp resonance appears only for polarization orthogonal to the grating line (transverse magnetic (TM) polarization), and it disappears when a nanoparticle is on the surface of the PC. The presence of nanoparticles on the PC surface causes either a shift in the reflection peak toward longer wavelengths, referred to as peak wavelength value (PWV) shift, or a drop in the magnitude of the peak, termed peak intensity value (PIV) reduction [17]. The PWV is important for dielectric nanoparticles and PIV reduction is more dominant for metal nanoparticles, though both effects exist in the two types of nanoparticles. Since no spectrometer is attached to the image sensor in SFPCEM, it can detect only PIV signals. Moreover, the raw signal in SFPCEM is weaker than that in PCEM since the signal originates from the entire emission spectrum of the LED, which contains the range of off-resonance. The reduced signal intensity should be compensated by processing images for higher contrast. In particular, compared with line imaging in PCEM, two-dimensional imaging offers several advantages such as high-speed image acquisition and a large FOV. In addition, the SFPCEM does not require an expensive scanning stage or spectrometer, resulting in a low-cost setup. The cost advantage can be crucial in adapting the SFPCEM device for portable and POC applications.



(a)



(b)



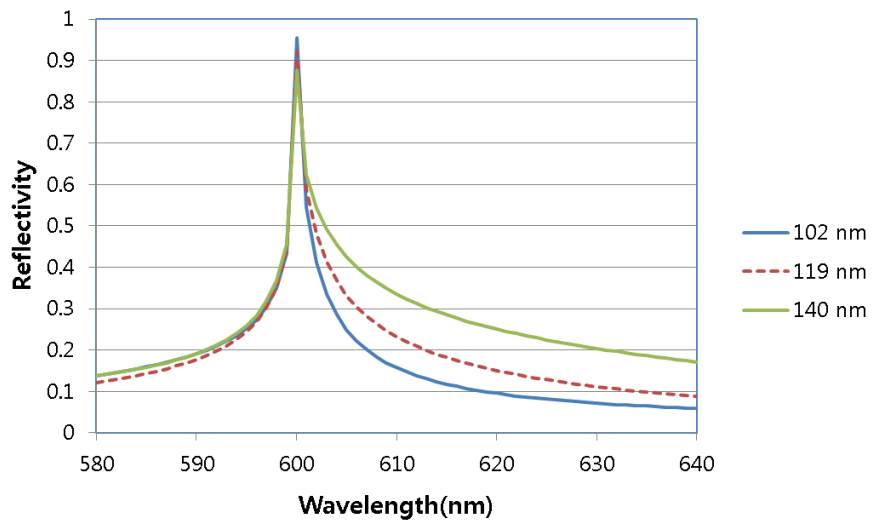
(c)

Fig. 1. (a) Schematic of the optical setup (b) and the PC substrate in SFPCEM. (c) The reflectivity of the PC substrate when t , h , a , and b are 51, 102, 260, and 140 nm, respectively.

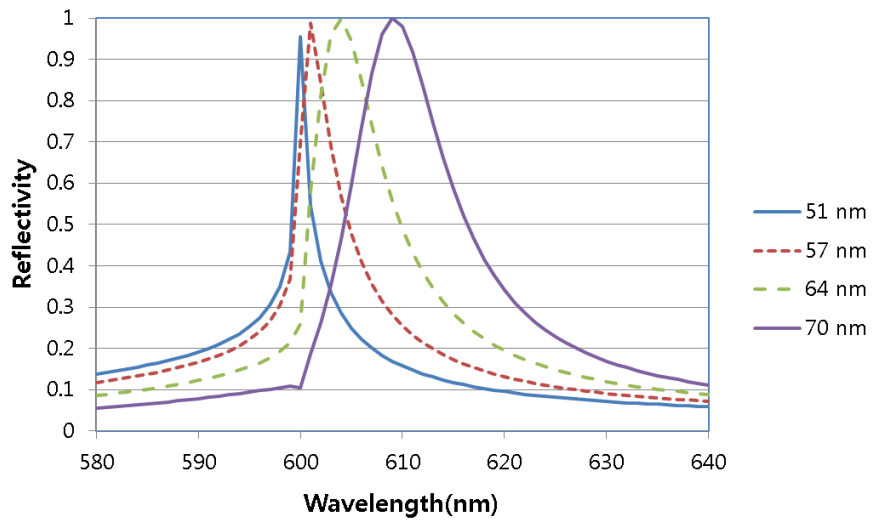
An analysis of a PC substrate used in SFPCEM was performed by using GSolver V5.2 [18]. In general, most researchers of PCEM use finite-difference time-domain (FDTD) [19] or rigorous coupled-wave theory (RCWT) [20] software for the two-dimensional (2D) and three-dimensional (3D) analysis of a PC. Although these softwares are accurate, they require more computing power and time compared with GSolver. GSolver also uses an RCWT algorithm, but it is more effective and fast for two-dimensional grating problems. In the tolerance analysis, many parameters of the PC structure and incident light are varied. In this study, parameters were varied and calculations were performed easily and accurately by using GSolver.

3. Results and Discussion

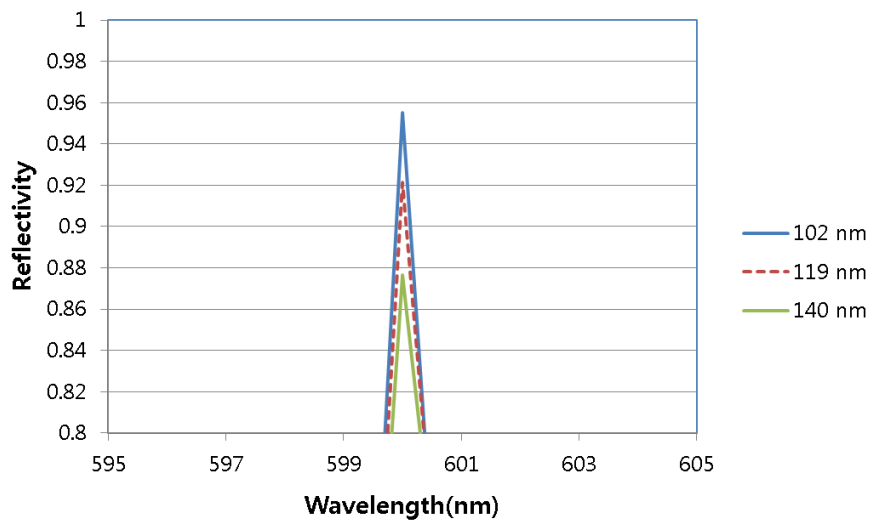
Several structural parameters were varied and the resulting change in the reflection spectrum and corresponding sensitivity were calculated. The first parameter group included the thicknesses of the SiO₂ and TiO₂ in the PC, which are denoted by h and t in Fig. 1(b). The parameters a and b in Fig. 1(b) were fixed at 260 and 140 nm, respectively. The polarization of the light was TM, implying that the electric field was perpendicular to the grating line. The calculation results are shown in Fig. 2. A change in the thickness of SiO₂ does not shift the resonance wavelength (Fig. 2(a)). A magnified view of the part of the curves near the peak in Fig. 2(a) is shown in Fig. 2(c), and it reveals different peak reflectivities. A thinner SiO₂ layer leads to a higher reflectivity in the thickness range considered. The reflectivity on the longer wavelength side of the resonance and the resonance linewidth increase with the SiO₂ thickness. For a 102 nm thick SiO₂ layer, the full width at half-maximum (FWHM) is about 3 nm, and it increases to 5 nm for a thickness of 140 nm. A change in the TiO₂ thickness causes more significant changes in the position and shape of the resonance peak, as evident in Fig. 2(b). As the TiO₂ thickness increases from 51 nm to 70 nm, the FWHM of the resonance peak increases from 3 nm to 13 nm, which amounts to a 300% increase for a 40% increase in the TiO₂ thickness. This increase is considerably greater than that for SiO₂, for which the resonance peak increased by only 60% for a 40% increase in thickness. The change in the TiO₂ thickness also shifts the resonance wavelength from 600 to 609 nm, apart from increasing the linewidth. Thus, the reflectivity spectrum is more sensitive to the thickness of TiO₂. In other words, the fabrication tolerance of the TiO₂ layer is tighter than that of the SiO₂ layer. For some applications, the TiO₂ thickness should be controlled accurately. For example, the SFPCEM setup can use a collimated LED such as M625L3-C1 [21] as a light source, for which the FWHM is about 18 nm. If the resonance linewidth of the PC is narrower than that of the light source, the PC can be sensitive to Au nanoparticles; however, the narrower linewidth would also lead to wastage of light energy outside the resonance peak. Therefore, the FWHM of the PC should not be significantly narrower than that of the LED. If the FWHM of the PC is half of that of the LED, the FWHM of the PC is about 9 nm, which corresponds to a TiO₂ thickness of about 64 nm. As for the 57 nm thick TiO₂ layer, the FWHM of the PC becomes 5 nm, which is about half of that of the 64 nm thick TiO₂ layer. The change in the TiO₂ layer thickness from 64 to 57 nm may lead to the halving of the energy efficiency and signal intensity in SFPCEM. The TiO₂ thickness should be controlled between 60 and 64 nm in order to maintain the energy efficiency at 75% of the maximum value. Since the TiO₂ layer is deposited by a sputtering machine, the accuracy and uniformity of the thickness can be ensured through careful tolerance management.



(a)



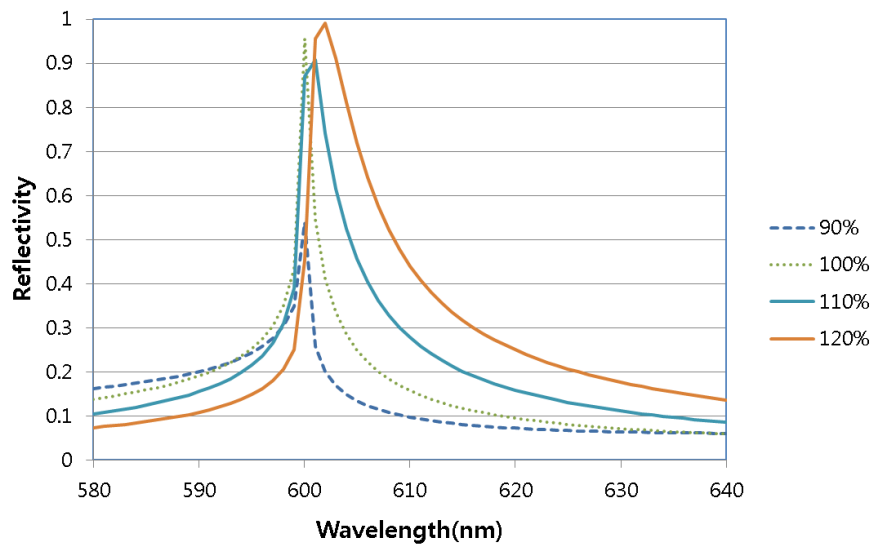
(b)



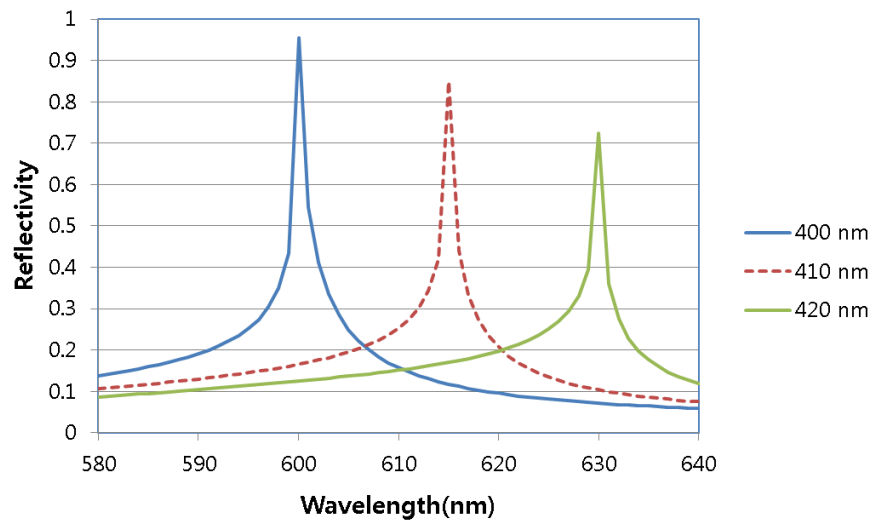
(c)

Fig. 2. Reflection spectra for different thicknesses of the (a) SiO₂ and (b) TiO₂ layers in the PC. In (a), the thickness of TiO₂ is 51 nm, and in (b), the thickness of SiO₂ is 102 nm. (c) A magnified view of (a) showing different peak reflectivities.

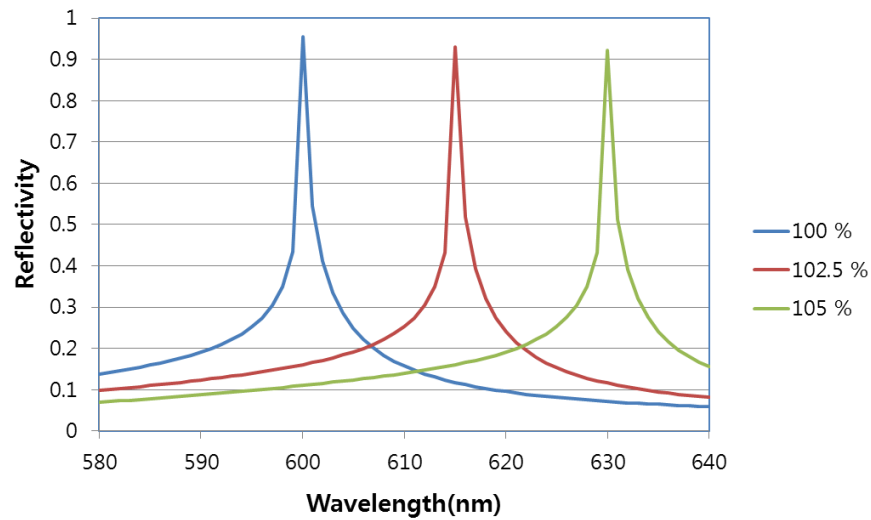
The next parameters investigated were the vertical and horizontal scales. The vertical scale refers to the sum of the SiO₂ thickness and TiO₂ thickness. If the vertical scale increases by 10%, then both SiO₂ and TiO₂ thickness increase by 10% simultaneously. The horizontal scale refers to the grating period of the PC with a fixed duty cycle. The results of calculations for the variation of the vertical scale, horizontal scale, and both scales are shown in Fig. 3(a), (b), and (c), respectively. For the reference structure indicated as 100% in Fig. 3(a), the thicknesses of SiO₂ and TiO₂ are 102 and 51 nm, respectively, and the parameters a and b in Fig. 1(b) are 260 and 140 nm, respectively. An increase in the vertical scale results in an increase in the reflectivity and its linewidth, as shown in Fig. 3(a). It is the combined effect of the increases in the thicknesses of TiO₂ and SiO₂. The linewidth increases with the vertical scale, which may be ascribed mainly to the increase in the thickness of TiO₂. A decrease in the vertical scale to 90% leads to a very rapid decrease in the reflectivity, indicating that the reference structure is around the edge of a sharp resonance condition with high reflectivity. The slight off-resonance resulting from the decrease in the vertical scale leads to the abrupt drop in reflectivity. Scaling in the horizontal direction mainly causes a shift in resonance toward long wavelengths and a slight decrease in the peak reflectivity, as evident in Fig. 3(b). The linewidth remains almost constant despite a change of about 5% in the grating period. Scaling in both vertical and horizontal directions shifts the resonance toward long wavelengths, with little change in the peak reflectivity (Fig. 3(c)). The amount of resonance shift is the same as the scaling factor, implying that a 5% increase in the scaling factor results in a 5% shift in the resonance wavelength. This is expected from the scaling property of the Maxwell equations, which remains unchanged if the structure and the wavelength scale in the same proportion. The slight difference in the peak intensity can result from a change in the refractive index of the material with wavelength. Therefore, this scaling property can be useful when adjusting the resonance wavelength of the PC to a new value or that of the light source.



(a)



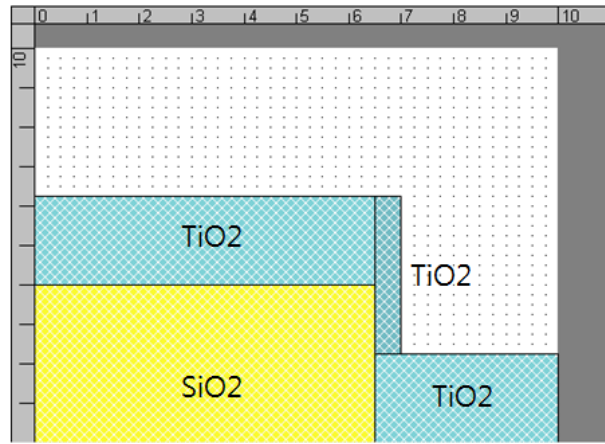
(b)



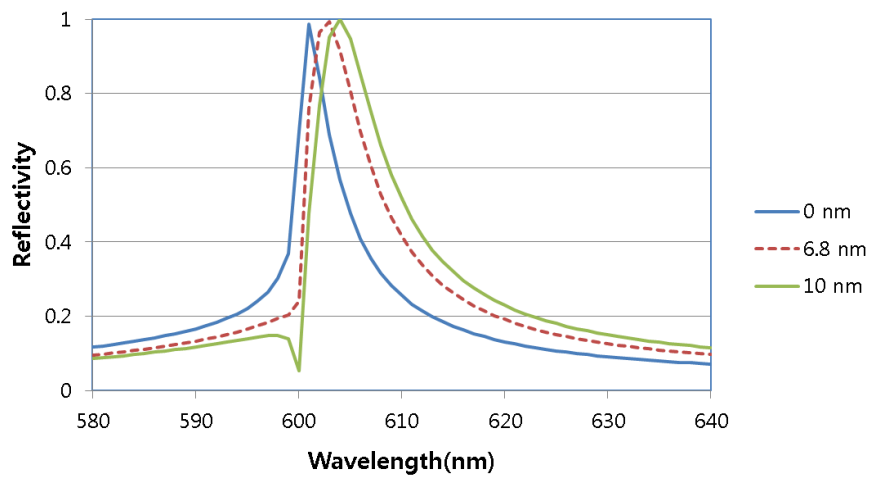
(c)

Fig. 3. Reflection spectrum obtained when (a) only the vertical scale, (b) only the horizontal scale (grating period), and (c) both vertical and horizontal scales are varied. For the reference structure indicated as 100%, the thicknesses of the SiO₂ and TiO₂ layers were 102 and 51 nm, respectively, and the parameters a and b in Fig. 1(b) were 260 and 140 nm, respectively.

The third parameter was related to a new type of PC with a TiO₂ coating on the sidewall of the grating; a cross-sectional profile of the PC is schematically shown in Fig. 4(a). Such sidewall coating can result from sputtered particles being incident on the substrate at an angle instead of the normal direction. A layer of TiO₂ was added to the sidewall without changing the other structural parameters. The additional TiO₂ layer increased the linewidth of the resonance peak, as shown in Fig. 4(b). In the simulation performed for the third parametric variation, the reference structure had 57 nm thick TiO₂ and 102 nm thick SiO₂ layers, as observed in Fig. 2(b). A 6.8 nm thick on the sidewall increased the peak linewidth from 5 to 7 nm. Therefore, the TiO₂ coating on the sidewall may affect the reflection spectrum strongly when it reaches 7 nm.



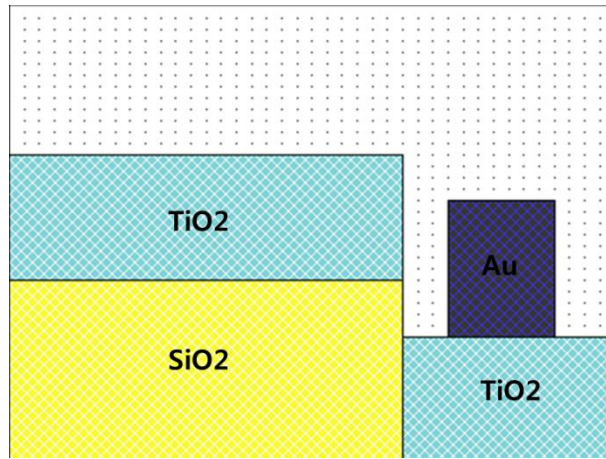
(a)



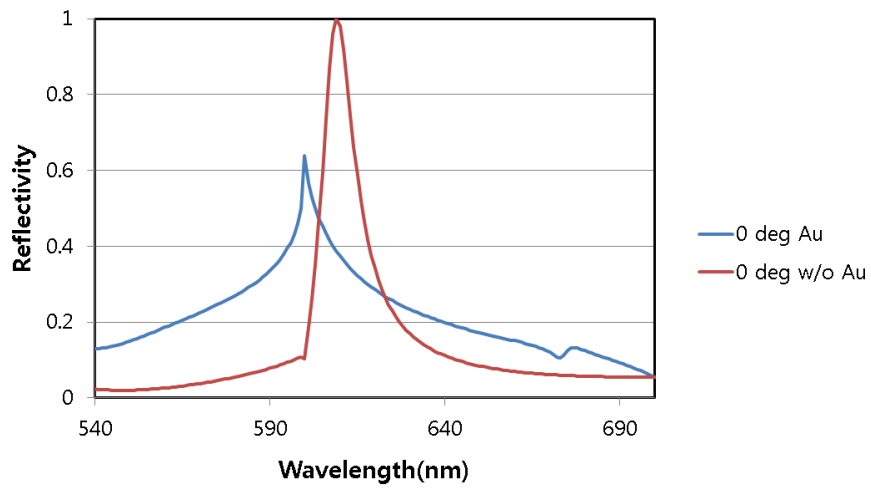
(b)

Fig. 4. TiO_2 coating on the sidewall of the PC: (a) a cross-sectional profile and (b) the reflection spectrum for various TiO_2 thicknesses.

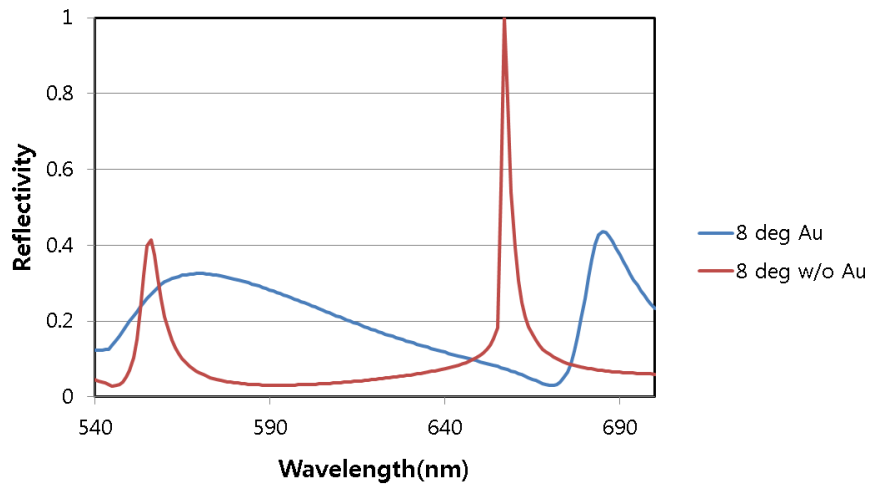
The fourth simulation was performed to examine the effect of a metal on the PC. Calculating the effect of nanoparticles on the PC requires 3D Maxwell equation solvers such as 3D FDTD or 3D RCWT. Although the GSolver can solve only 2D problems, by simulating metallic nanowires in the PC, it can provide insights into possible scenarios in the event of the PC containing metal structures. The structure used in the simulation is shown in Fig. 5(a); a Au nanowire with a height and width of 90 and 70 nm was placed in a groove on the PC. The calculation results are presented in Fig. 5(b) and (c). The reflectivity of the PC decreased significantly in the presence of the Au nanowire. Fig. 5(c) shows the results for the case where light was incident at an angle of 8° . The difference between the PC with a Au nanowire and the PC without a Au nanowire is greater at the angle of 8° compared with that at 0° .



(a)



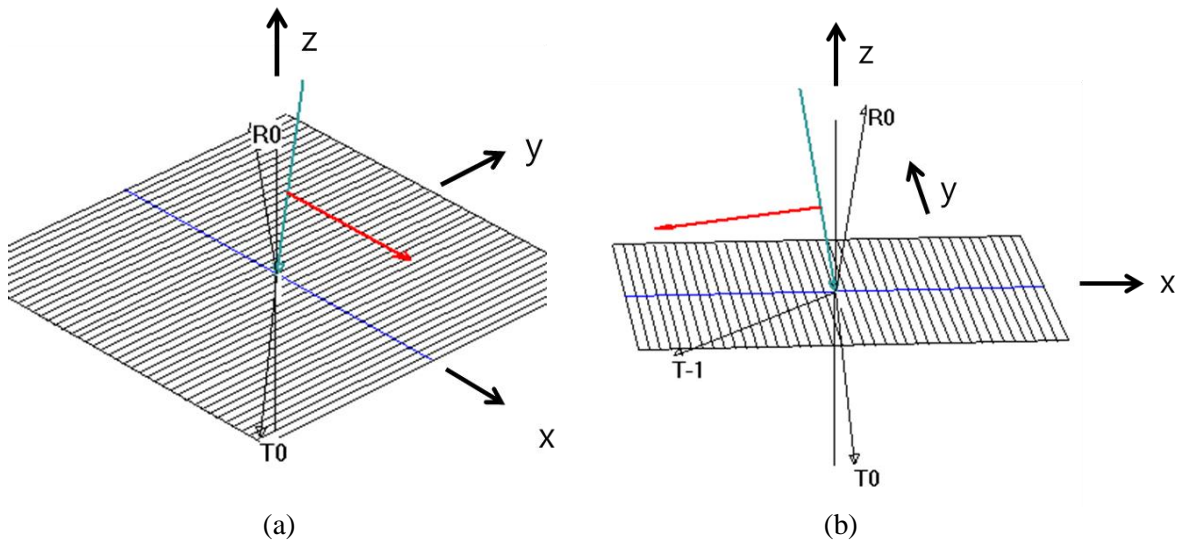
(b)



(c)

Fig. 5. (a) Cross-sectional profile of the PC with a Au nanowire in its periodic structure and reflection spectra at light incidence angles of (b) 0° and (c) 8° . The height and width of the nanowire were 90 and 70 nm, respectively.

Finally, the angle dependency of the PC was investigated by changing the angle at which light was incident on the PC. So far, TM polarization was maintained in the simulations since polarization parallel to the grating line (TE polarization) did not show resonance or a significant change in the presence of the Au nanowire. The incidence angle was assumed to be 0° , except in Fig. 5(c). The optical setup (shown in Fig. 1) contained a microscope objective lens for imaging the nanoparticles on the PC. Since a microscope objective lens has finite numerical aperture, a considerably large portion of the light is incident on the PC at an angle. If the numerical aperture of the lens is 0.25, the largest incidence angle is 14° . Therefore, investigating the incident light angle dependency of the PC is important for the tolerance analysis of SFPCEM. Prior to the calculation, an understanding of the tilt angle for a PC is necessary. The incident light can be tilted in two ways, as shown in Fig. 6(a) and (b): in a direction normal to the grating line, which is the $-x$ -direction (Fig. 6(a)), and in the direction parallel to the grating line, which is the $-y$ -direction (Fig. 6(b)). In both cases, the polarization is maintained in the TM mode. The incidence angles in the two cases are represented by θ and θ' , respectively. The simulation results for the titled incidence angles are shown in Fig. 6(c) and (d). The behavior of the reflectivity spectrum obviously depends on the tilt direction. Tilting in θ -direction causes a large shift in the resonance peak apart from split the peak into two. For the 8° tilt, the peak at 609 nm splits into peaks at 657 and 555 nm. The sensitivity of the resonance to the angle is about 6.0 nm/deg. The peak on the long wavelength side also becomes narrower with an increase in the incidence angle. By contrast, tilting in the θ' -direction results in little change in the resonance peak shape and resonance wavelength. The resonance peak shifts from 609 nm to 607 nm as θ' increases from 0° to 8° . This distinctive dependence of the reflectivity spectrum behavior on the tilt direction may result in peculiar imaging in SFPCEM. The finite bandwidth of the light source (such as LEDs) limits the practical numerical aperture of the imaging optics. If half the bandwidth of an LED such as M625L3-C1 is 9 nm, the corresponding angular breadth in the θ -direction is only 1.5° and the numerical aperture is 0.025 for the angular sensitivity in the θ -direction. While the numerical aperture in the θ' -direction is 0.25, the numerical aperture in the θ -direction is only one-tenth of that. Since the numerical aperture determines the image resolution [22], the resolution in the θ -direction is 10 times worse than that in the θ' -direction. The effect in the final image of nanoparticles obtained by SFPCEM is an image elongated in the direction perpendicular to the grating line. This phenomenon was actually observed in a SFPCEM image, which is shown in Fig. 7. It is interesting that tolerance analysis can explain the peculiarity of the SFPCEM image.



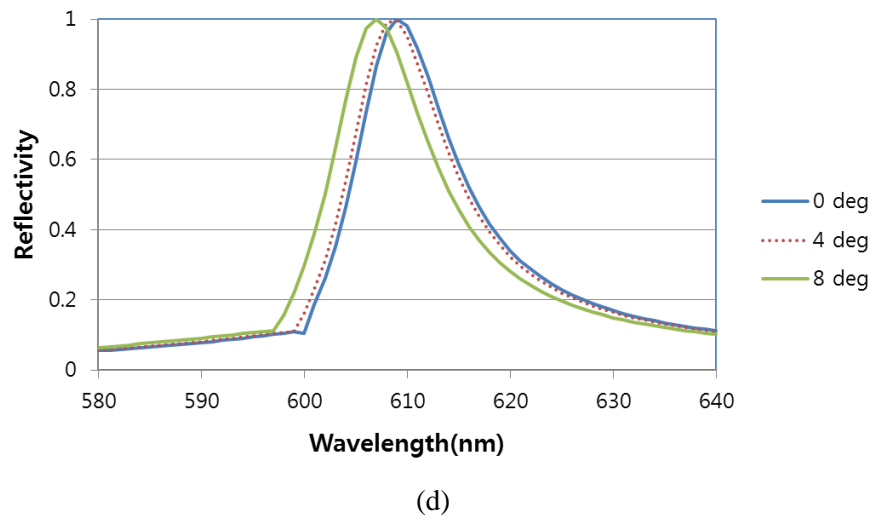
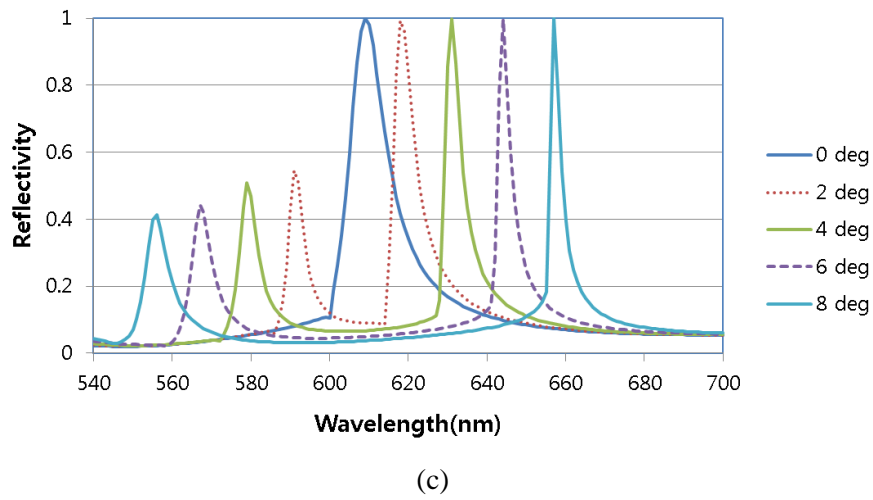


Fig. 6. Dependence of the reflectivity on the incidence angle was investigated. The orientations of tilt angles (a) θ and (b) θ' are illustrated where the red arrows indicate the direction of the electric field or the polarization. Reflectivity spectra for various values of (c) θ and (d) θ' are also shown.

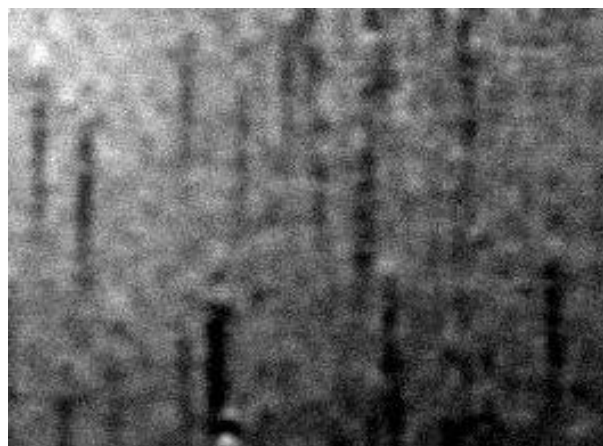


Fig. 7. SFPCEM image of Au nanoparticles with dimensions of 49 μm \times 36 μm . The grating is horizontal.

4. Conclusions

A tolerance analysis of a PC substrate used in SFPCEM was conducted. SFPCEM is a modified version of PCEM for viewing nanoparticles without an expensive spectrometer or scanning stage. We varied various structural parameters of the PC substrate and calculated the change in its reflectivity spectrum in order to calculate the tolerance and sensitivity of the PC performance to the parameters.

First, the thicknesses of SiO₂ and TiO₂ were changed. As the TiO₂ thickness increased from 51 to 70 nm, the FWHM of the resonance peak increased from 3 to 13 nm. The FWHM increased by 300% when the TiO₂ thickness increased by 40%. The change in the FWHM with the TiO₂ thickness was much greater than that with the SiO₂ thickness; the increase in the FWHM was only 60 % for a 40 % increase in the SiO₂ thickness.

Second, the PC structure was scaled in various proportions in the vertical direction, horizontal direction, and both directions. An increase in the vertical scale resulted in an increase in the reflectivity and its linewidth. The effect of the TiO₂ thickness was greater than that of the SiO₂ thickness. For the scaling in the horizontal direction and in both directions, the reflectivity spectrum behavior was similar and the resonance showed a shift, with the shift being in the same proportion as the scaling factor. In particular, the horizontal scaling resulted in reduced peak reflectivity for large scaling factors.

The third parametric variation was applied to a new type of PC with a TiO₂ coating on the sidewall of the grating. An additional TiO₂ coating on the sidewall increased the resonance linewidth. A 6.8 nm thick TiO₂ coating on the sidewall increased the peak linewidth from 5 to 7 nm.

Fourth, simulations were performed to examine the effect of metal nanoparticles on the PC. When a Au nanowire with a height and a width of 90 and 70 nm was placed in a groove of the PC, the reflectivity of the PC decreased significantly. The difference between the PC with a Au nanowire and the PC without a nanowire increased at an incidence angle of 8° compared with that at an incidence angle of 0°.

Finally, the angle dependency of the PC was investigated by changing the angle at which light was incident on the PC. The behavior of the reflectivity spectrum showed obvious dependence on the tilt direction. Tilting in the direction perpendicular to the grating caused a large shift in the resonance peak apart from splitting the peak into two. For the incidence angle of 8°, the peak at 610 nm was split into peaks at 657 and 555 nm. The sensitivity of the resonance to the incidence angle was 12 nm/deg. By contrast, tilting in the grating direction resulted in little change in the resonance peak shape and resonance wavelength. The resonance peak shifted from 609 nm to 607 nm as θ increased from 0° to 8°. This distinctive tilt dependence of the resonance peak may result in elongated images of nanoparticles in SFPCEM. The finite bandwidth of the light source limits the practical numerical aperture in the direction perpendicular to the grating. Since the numerical aperture determines the resolution, the resolution in the θ -direction is considerably worse than that in the θ -direction. This results in the image of nanoparticles being elongated in the direction perpendicular to the grating line. This phenomenon was actually observed in a real SFPCEM image.

The tolerance analysis performed in this study can be helpful in many ways such as the optimization of PC substrates for use in SFPCEM and the estimation of the fabrication tolerance of PC substrates. Furthermore, it can help in identifying the reasons for peculiarities in SFPCEM images.

5. Acknowledgment

The author sincerely thanks Jong-Ho Jeon for lending the GSolver software.

References

- [1] K. T. Thurn, T. Paunesku, A. Wu, E. M. Brown, B. Lai, S. Vogt, J. Maser, M. Aslam, V. Dravid, R. Bergan and G. E. Woloschak, *Small*, 2009, 5, 1318–1325.
- [2] D. Ishii, K. Kinbara, Y. Ishida, N. Ishii, M. Okochi, M. Yohda and T. Aida, *Nature*, 2003, 423, 628–632.
- [3] R. A. Sperling, P. R. Gil, F. Zhang, M. Zanella and W. J. Parak, *Chem. Soc. Rev.*, 2008, 37, 1896–1908.
- [4] P. M. Winter, A. M. Morawski, S. D. Caruthers, R. W. Fuhrhop, H. Zhang, T. A. Williams, J. S. Allen, E. K. Lacy, J. D. Robertson, G. M. Lanza and S. A. Wickline, *Circulation*, 2003, 108, 2270–2274.
- [5] J. N. Anker, W. P. Hall, O. Lyandres, N. C. Shah, J. Zhao and R. P. Van Duyne, *Nat. Mater.*, 2008, 7, 442–453.
- [6] A. Mitra, B. Deutsch, F. Ignatovich, C. Dykes and L. Novotny, *ACS Nano*, 2010, 4, 1305–1312.
- [7] K. M. Mayer, F. Hao, S. Lee, P. Nordlander and J. H. Hafner, *Nanotechnology*, 2010, 21, 255503.
- [8] M. F. Miller, B. P. Masters and M. E. Lundstrom, *US Pat.*, 2007, US 7300631 B2.
- [9] Y. Wang, H. Chen, S. Dong and E. Wang, *J. Chem. Phys.*, 2006, 125, 44710.
- [10] L. Cognet, C. Tardin, D. Boyer, D. Choquet, P. Tamarat and B. Lounis, *Proc. Natl. Acad. Sci. U. S. A.*, 2003, 100, 11350–11355.
- [11] M. R. Lee and P. M. Fauchet, *Opt. Lett.*, 2007, 32, 3284–3286.
- [12] A. Kotnala, D. DePaoli and R. Gordon, *Lab Chip*, 2013, 13, 4142–4146.
- [13] S. Nie and S. R. Emory, *Science*, 1997, 275, 1102–1106.
- [14] B. T. Cunningham, B. Lin, J. Qiu, P. Li, J. Pepper and B. Hugh, *Sens. Actuators, B*, 2002, 85, 219–226.
- [15] R. Vedula, G. Daaboul, A. Reddington, E. Ozkumur, D. A. Bergstein and M. S. Unlu, *J. Mod. Opt.*, 2010, 57, 1564–1569.
- [16] W. Chen, K. D. Long, M. Lu, V. Chaudhery, H. Yu, J. S. Choi, J. Polans, Y. Zhuo, B. A. Harley and B. T. Cunningham, *Analyst*, 2013, 138, 5886–5894.
- [17] Y. Zhuo, H. Hu, W. Chen, M. Lu, L. Tian, H. Yu, K. D. Long, E. Chow, W. P. King, S. Singamaneni and B. T. Cunningham, *Analyst*, 2014, 139, 1007
- [18] <http://www.gsolver.com/>
- [19] A. Taflove and S. C. Hagness, 2000 *Computational Electrodynamics: The Finite-Difference Time-Domain Method*, 3rd ed. (Boston, Artech House Publishers)
- [20] M. G. Moharam and T. K. Gaylord, *J. Opt. Soc. Am.*, 1981, 71, 811–818
- [21] <https://www.thorlabs.com/thorproduct.cfm?partnumber=M625L3-C1>
- [22] J. E. Greivenkamp, 2004 *Field Guide to Geometrical Optics* (SPIE Field Guides vol FG01) (Bellingham, WA:SPIE Optical Engineering Press) p 88